



Probabilistic resilience assessment framework for cyber-physics multi-microgrids systems considering uncertainty

Qiaoyuan Kou^a, Hongli Zhang^{b,*}, Cong Wang^b, Yue Meng^b

^a School of Electrical Engineering, Xinjiang University, Urumqi, Xinjiang, China

^b School of Intelligence Science and Technology, Xinjiang University, Urumqi, Xinjiang, China

ARTICLE INFO

Keywords:

Probabilistic resilience assessment
Cyber-Physical Multi-Microgrids
Seismic disasters
System functional model
Uncertainty

ABSTRACT

Breakthroughs in power electronics, advanced metering, and communication technologies have driven the development of cyber-physical multi-microgrids (CPMMGs). Although CPMMGs have significant advantages in integrating large-scale distributed generation, they face more complex safety risks during extreme events such as earthquakes due to the deep cyber-physical coupling characteristics. Current seismic resilience assessments mostly use a single numerical value after the system has fully recovered under a specific earthquake magnitude, making it difficult to quantify the uncertainties in the performance changes throughout the damage-recovery process of CPMMGs. Considering the limitations of insufficient exploration on the cyber-physical coupling mechanism of CPMMGs, reliance on static one-dimensional indicators, and failure to integrate multiple uncertainties, this paper constructs a probabilistic resilience analysis framework for CPMMGs by comprehensively considering uncertain factors such as seismic hazards, renewable energy, and component maintenance. The specific innovations and contributions are as follows: First, a cross-domain fault propagation model is established to reveal the impact of the cyber-physical coupling mechanism on system resilience; second, a resilience index and post-disaster response model including topological attributes and operational attributes are constructed to adapt to the deep cyber-physical integration characteristics of CPMMGs; third, a probabilistic resilience assessment framework for the entire damage-recovery stage after an earthquake is proposed to fully describe the dynamic evolution process of system resilience. The study verifies the application of the framework through the CPMMGs structure based on the improved IEEE RBTS, which can provide important theoretical and practical support for the disaster-resistant planning of CPMMGs.

1. Introduction

The breakthroughs in power electronics, advanced metering, and communication technologies have propelled the collaborative networking of microgrid clusters, resulting in the creation of the CPMMGs architecture [1], which supports the integration of large-scale Distributed Generation (DG). The CPMMGs represent a typical form of the power system's evolution towards intelligence and sustainability [2]. Extreme weather events, such as earthquakes and typhoons, pose significant challenges to the safe and stable operation of power systems [3,4]. Similarly, as vital components of critical infrastructure, CPMMGs is susceptible to such disruptive events, thereby establishing resilience management as a pivotal focus of academic research.

Unlike traditional power systems, which rely on centralized architectures for generation, transmission, distribution, and consumption [5],

CPMMGs utilize cyber-physical fusion technologies to create distributed topologies that support multi-mode collaborative operation of microgrid (MG), both in islanded and grid-connected modes [6]. The fault response of CPMMGs is more flexible, and their topological reconfiguration capabilities surpass those of traditional power systems [2]. However, their unique flexible operation mechanisms and cyber-physical interactions significantly increase the complexity of modeling. Despite the advantages of CPMMGs in supply reliability and demand response, the cyber-physical coupling exacerbates safety risks during extreme events. The spatial and temporal randomness of extreme disasters, the intermittency of renewable energy, and the uncertainty of equipment repair all directly affect the multi-stage resilience evolution of CPMMGs. Current seismic resilience assessments of power systems often use a single numerical value representing the system's full recovery after a specific earthquake magnitude [7,8], making it difficult to quantify the uncertainty of CPMMGs' damage-recovery process. This paper proposes a

* Corresponding author.

E-mail address: zhl@xju.edu.cn (H. Zhang).

Abbreviation	
CPMMGs	Cyber-Physical Multi-Microgrids
DG	Distributed Generation
MG	Microgrid
ICT	Information and communication technologies
WT	Wind turbine
PV	Photovoltaics
ESS	Energy storage system
DE	Diesel engine
PCC	Point of Common Coupling
CB	Circuit breakers
MGCC	Microgrid control centers
CEMS	Community energy management system
MC	Microcontroller
LC	Load controller
CBC	Circuit breaker controller
MMGs	Multi-Microgrids
IO	Islanding operation
JO	Joint operation
SO	Shutdown operation
PGA	Peak ground acceleration
SA	Spectral acceleration
<i>Nations</i>	
\mathcal{M}	Multi-layer network of CPMMGs
\mathcal{Y}	Set of network layers
$\overrightarrow{\mathcal{G}}$	Ordered list of cyber layer and physical layer
\mathcal{Z}	Bipartite network
G_C	Network of the cyber system
G_P	Network of the physical system
V_C	Sets of nodes for the G_C
V_P	Sets of nodes for the G_P
$E_{C,P}$	Set of Links between the G_C and the G_P
$a^{[.,.]}$	Adjacency matrices
\mathcal{A}	Supra-adjacency matrix of CPMMGs
$\varphi_{i,j}^C$	Working state of the cyber node i coupled with the physical node j
P_j	Current loads at physical node j
γ	Interaction factor
P_{DGj}	Output power of the j -th DG
$V_{P,DG}$	Set of DG nodes in the G_P
$V_{C,DG}$	Set of cyber nodes for DGs in the G_C
v	Wind speed
$v_{ci}, v_{co}, v_{rated}$	The cut-in wind speed, cut-out wind speed and rated wind speed
k_{wind}, λ_{wind}	The shape and scale parameters of Weibull distribution with wind speed
P_{rated}^{WT}	Rated output power of wind turbine
r	Solar intensity
r_{max}	Maximum solar intensity
α_{PV}, β_{PV}	The parameters of the beta distribution with solar radiation intensity
Ar	Area of the solar panel
K_r	Threshold of solar radiation intensity
SOC	Charge of the ESS under simulation
τ	Intrinsic discharge rate
P_{ESSc}, P_{ESSd}	The charge and discharge power o
F_{ESSc}, F_{ESSd}	The charge and discharge state
δ_c, δ_d	The charge and discharge power efficiencies
P_{DE}	Output power of the diesel engine
$P_{DE}^{max}, P_{DE}^{min}$	The minimum and maximum output power of DE
$a_{l,m}$	Importance of the l -th load in the m -th MG
$LS_{l,m}(t)$	The l -th user load to be curtailed in the m -th MG
$N_{l,m}$	Load number in the m -th MG
$LS_{l,m}$	The l -th load to be curtailed in the m -th MG
M_{IO}	Set of MGs operating in IO mode within CPMMGs
M_{JO}	Set of MGs operating in JO mode within CPMMGs
L_m	Set of users load in the m -th MG
$P_{WT,m}$	Output power of the WT in the m -th MG
$P_{PV,m}$	Output power of the PV in the m -th MG
P_m^{ex}	Power exchange between MGs
L_m^{tot}	all the load demands in the MG
$L_{l,m}$	Load demand of the l -th user in the m -th MG
p_{shot}, p_{excess}	The shot and excess power of MG
$p_{out,ex}, p_{in,ex}$	The surplus and deficit of power for MG
N_{JO}	Number of MGs operating in JO mode
IM	Richter magnitude scale
D	Epicentral distance
μ_e, σ_e	The mean value and the standard deviation lognormal probability distributions of fragility
t_e	Repair time of equipment
t_{e^c}, t_{e^p}	The repair time for component in the cyber system the physical system
T_{MG_m}	Recovery durations for the m -th MG
$N_{e,damme}^C$	Number of damage node in the cyber system
$N_{e,damge}^P$	Number of damage node in the physical system
T_S	Recovery time of CPMMGs
M	Set of all MGs in the CPMMGs
η_{Tr}^P	Residual power path ratio in physical network
η_{Tr}^C	Residual information transmission ratio in cyber network
η_{Tr}	Power delivery rate
η_s	Power supply reliability rate
$P_{supplied}$	Actual supplied power in CPMMGs
P_{demand}	Power demand of users in CPMMGs
Q	System functionality
Q_{res}	Residual functionality
R_r	System robustness index
R_t	Recovery duration
R_{IM}	Seismic resilience index
R_{IM}^{tar}	Target resilience under the seismic intensity level IM .
$k_{R IM}, \lambda_{R IM}$	The shape parameter and scale parameter of the truncated Weibull distribution
θ_0, θ_1	Regression parameters
\mathcal{V}	Annual exceedance probability
\mathcal{V}_{y-year}	Life-cycle exceedance probability

probabilistic resilience analysis framework for CPMMGs, taking into account uncertainties such as seismic disasters, renewable energy sources, and component repairs, which is crucial for disaster planning in CPMMGs.

Current research on CPMMGs mainly focuses on multi-modal flexible operational mechanisms, fault response strategies and reliability of cyber system. In terms of system stability, Zhao et al. [9] proposed a

hierarchical distributed damping control strategy to mitigate multi-modal oscillations in wind–solar–storage MGs, ensuring smooth transitions between grid-connected and islanded modes. Wang et al. [10] introduced a data-driven voltage regulation method to ensure stable multi-microgrid (MMG) operation. Mansouri et al. [11] developed a deep reinforcement learning-based cloud–fog computing framework for real-time energy management. For fault response,

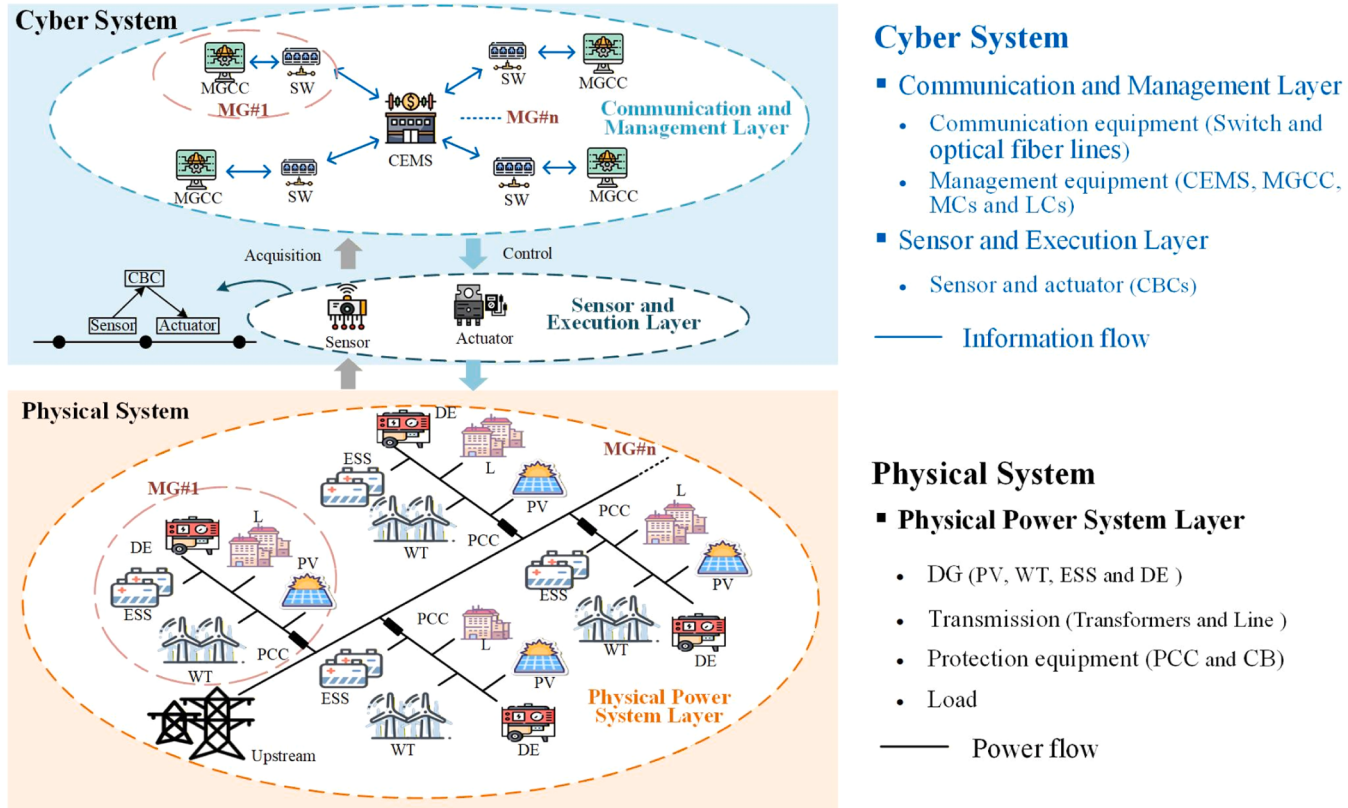


Fig. 1. Cyber-physical system structure of CPMMGs.

Mumtaz et al. [12] applied unscented Kalman filters for fault detection, classification, and localization in MGs with multiple distributed sources. Shaker et al. [13] designed adaptive multi-mode control strategies to suppress voltage fluctuations caused by faults. Ward et al. [14] proposed an innovative inverter control scheme to support black start capability under transient faults. Regarding reliable cyber system, Wang et al. [15] and Barani et al. [16] modeled information link failures and conducted reliability analysis for MGs. Xiao et al. [17] designed a communication network architecture resistant to cyber-attacks. Although these studies effectively enhance MG stability and address component-level faults, they often focus on isolated analysis of either the cyber or physical domain. Research into cross-domain fault propagation due to cyber-physical integration in CPMMGs remains limited.

Other scholars investigated responses to specific disasters. Ti et al. [18] revealed spatiotemporal vulnerabilities of power systems during typhoons. Gautam et al. [19] used energy not supplied metrics to describe performance degradation in distribution networks under storm conditions. Ferrario et al. [20] and Amani-Jouneghani et al. [21] used topological indicators and vulnerability curves, respectively, to assess seismic impacts on distribution networks. Zhang et al. [22] conducted seismic risk assessment using a DC optimal power flow model. Farzin et al. [23] and Jalilpoor et al. [24] optimized outage management and network configuration to enhance MG resilience. Younesi et al. [25] evaluated the resilience of large-scale power systems with MGs against natural disasters. Hou et al. [26] proposed a robust optimization framework to improve distribution network resilience under typhoon events. In summary, existing resilience studies are mostly limited to power systems and static, single-dimensional evaluation approaches. These methods fail to fully capture the dynamic evolution of CPMMG resilience in post-earthquake scenarios under uncertainty.

Extreme disasters introduce considerable uncertainty in power systems. Probabilistic methods offer significant advantages in analyzing such uncertainty and are widely used in disaster risk assessment.

Sánchez-Pozo et al. [27] analyzed joint probability distributions of extreme weather to quantify aging risks of renewable energy components like PV panels and wind turbine transformers. Nazemi et al. [28] and Gao et al. [29] established probabilistic models linking disaster intensity to overhead line failures, laying the foundation for dynamic resilience evaluation. Liu et al. [30] calculated the probabilistic damage distribution of transmission tower-line systems during earthquakes. Bessani et al. [31] studied how component performance variability under extreme weather affects distribution network topology from a probabilistic perspective. Liu et al. [32] used Monte Carlo methods to assess seismic resilience of substations and associated influencing factors. Overall, probabilistic methods enable quantitative resilience evaluation by linking disaster intensity distributions, equipment failure probabilities, and system functionality losses. In the case of CPMMGs, resilience evaluation must also consider cyber systems (e.g., sensors, controllers, data links), as their failures can cascade into the physical layer during earthquakes. This introduces significant challenges to seismic resilience and uncertainty analysis for CPMMGs.

Although much research has been conducted on CPMMG fault responses, robust operation mechanisms and reliability, most studies isolate the cyber and physical domains without fully exploring their coupling's impact on resilience. During extreme events like earthquakes, failures in physical components (e.g., transmission lines, substations) and cyber systems (e.g., communication links, controllers) may interact via cross-domain coupling, triggering cascading failures and expanding system-wide disruptions. However, existing studies lack systematic modeling of such dynamic fault propagation processes and cannot effectively explain the evolution path of post-earthquake failures. Furthermore, current resilience assessments are often limited to single static indicators, which are insufficient for capturing the full damage-to-recovery performance trajectory of CPMMGs. While some research has developed multi-stage resilience evaluation frameworks for multi-energy systems [33], these models often fail to incorporate

multi-source uncertainties, such as earthquake intensities, equipment fragility, and recovery resources, making them inadequate for comprehensive probabilistic resilience analysis and seismic decision optimization. This paper makes the following key contributions:

- (1) Establishing a fault propagation model for CPMMGs by analyzing the coupling between cyber and physical systems, thus addressing the research gap on cyber-physical interactions.
- (2) Proposing a post-earthquake response model for CPMMGs and developing resilience indicators that integrate both topological and operational characteristics.
- (3) Introducing a probabilistic framework for evaluating the damage-recovery evolution of CPMMGs at post-earthquake, enabling comprehensive multi-stage resilience analysis under uncertainty.

The following sections provide a comprehensive overview of the probabilistic seismic resilience analysis process for CPMMGs. Section 2 presents the system model, seismic fragility model, and post-earthquake recovery processes for CPMMGs. Section 3 introduces the framework for seismic resilience assessment and analysis. Section 4 demonstrates the application of the framework using a modified IEEE RBTS-based CPMMGs system. Section 5 presents the conclusions and discussions of the study, and Section 6 summarizes the limitations of this work and outlines future research directions.

2. Modeling and post-earthquake operation of CPMMGs

2.1. Operational model of CPMMG

The CPMMGs represents the highly coupled nature of the cyber-physical system through the sophisticated interconnection of physical-electrical components, enabled by advanced information and communication technologies (ICT). As illustrated in Fig. 1, the system can be divided into three layers:

- Physical Power System Layer: This layer comprises essential electrical components, including transformers, line, DG units, including wind turbines (WT), photovoltaic (PV) systems, energy storage systems (ESS) and diesel engines (DE), protection equipment, such as Point of Common Coupling (PCC) and circuit breakers (CB), and loads. It is responsible for power supply and distribution.
- Sensor and Execution Layer: Equipped with measurement and control devices, this layer monitors the system's status in real time and executes upper-level control commands to ensure stable system operation.
- Communication and Management Layer: This layer is further divided into communication equipment and management equipment. The communication equipment facilitates data transmission through devices such as switches and optical fiber line. The management layer includes the main controller, the microgrids control centers (MGCC), and the community energy management system (CEMS), which oversee the system's overall regulation. The main controller includes microcontrollers (MCs), load controllers (LCs), and circuit breaker controllers (CBCs) for DERs, among others, and is responsible for precise control of local devices. The MGCC focuses on the internal management of the MG, while the CEMS optimizes energy scheduling between MGs.

Fig. 1 illustrates the Sensor and Execution Layer as a bridge between the Physical Power Layer and the Communication and Management Layer. The Physical Power Layer supplies power to local sensors and actuators, which are responsible for collecting operational status and measurement data from physical devices. The MGCC and the CEMS in the Communication and Management Layer are powered by proximity and equipped with backup power to ensure system reliability.

The CPMMGs architecture is divided into physical and cyber

systems. The Physical Power System Layer constitutes the physical infrastructure. Acting primarily as conduits for data flow, the Sensor and Execution Layer and the Communication and Management Layer are not directly involved in transmitting electrical power. Consequently, these two layers are collectively identified as the cyber system

2.1.1. Cyber-Physical interdependence analysis

Based on the multi-layer network theory in complex networks [34], CPMMGs can be modeled as $\mathcal{M} = (Y, \vec{G}, \mathcal{G})$, where Y represents the set of network layers, \vec{G} denotes the ordered list of the cyber layer and the physical layer. $\vec{G} = (G_C, G_P)$, G_C is the network of the cyber system, G_P is the network of the physical system, and \mathcal{G} is a bipartite network across the cyber network and the physical network, denoted by $\mathcal{G}_{C,P} = (V_C, V_P, E_{C,P})$. Herein, V_C and V_P are the node sets of the cyber network and the physical network, respectively, and $E_{C,P}$ is the interconnection, representing the links between the cyber network and the network system. The node set of the cyber network is defined as $V_C = \{(i, C) | i \in \{1, 2, \dots, N_C\}\}$, and the node set of the physical network is defined as $V_P = \{(i, P) | i \in \{1, 2, \dots, N_P\}\}$. The cyber network G_C and the physical network G_P are determined by adjacency matrices $a^{[C,C]}$ and $a^{[P,P]}$ respectively. The bipartite network \mathcal{G} for the interaction between the cyber network and the physical network is represented by the $N_C \times N_P$ incidence matrix $a^{[C,P]}$ and the $N_P \times N_C$ incidence matrix $a^{[P,C]}$. The incidence matrix $a^{[C,P]}$ has elements as follows:

$$a_{ij}^{[C,P]} = \begin{cases} 1, & \text{if } (i, C) \text{ is linked to } (j, P) \\ 0, & \text{otherwise} \end{cases} \quad (1)$$

The interactions between the two-layer networks of CPMMGs can be described using a supra-adjacency matrix \mathcal{A} :

$$\mathcal{A} = \begin{pmatrix} a^{[C,C]} & a^{[C,P]} \\ a^{[P,C]} & a^{[P,P]} \end{pmatrix} \quad (2)$$

The working state of a cyber node is a decision variable, represented by a Boolean value, $\varphi_{ij}^C \in \{0, 1\}, i \in V_C$. If there is an information flow between the uncontrol node and the control node, it is denoted as 1; otherwise, it is denoted as 0. Since the cyber equipment is powered by proximity [18], its working status is directly affected by the state of the physical node.

$$\varphi_{ij}^C = \begin{cases} 1, & P_j \geq \gamma P_{j,0} \\ 0, & P_j < \gamma P_{j,0} \end{cases}, \quad j \in V_P, i \in V_C \quad (3)$$

where φ_{ij}^C indicates the working status of the cyber node i powered by physical j nodes. If $\varphi_{ij}^C = 1$, it signifies that the node is being powered normally. P_j and $P_{j,0}$ represent the current and initial loads at physical node j , respectively. γ is the interaction factor that reflects the influence of the physical network on the cyber network.

In CPMMGs, if cyber node fails, the coupled physical node will lose control and be considered as failed. The operational status of the DG is centrally monitored and regulated by the MC. When the system encounters a major disturbance, if the MC fails, the DG will lose control commands, resulting in a failure to maintain normal power output. This relationship can be expressed as

$$\varphi_{i,DGj}^C P_{DGj}^{\min} \leq P_{DGj} \leq \varphi_{i,DGj}^C P_{DGj}^{\max}, i \in V_{C,DG}, j \in V_{P,DG} \quad (4)$$

where P_{DGj} , P_{DGj}^{\min} and P_{DGj}^{\max} are the generated power, and minimum and maximum output limits of DG node j respectively; $\varphi_{i,DGj}^C$ indicates the control node in the cyber network that governs DGj ; $V_{P,DG}$ denotes the set of DG nodes in the physical network; $V_{C,DG}$ represents the set of cyber nodes for DGs in the cyber network.

2.1.2. MMGs model

Wind power generation is directly influenced by wind speed, which exhibits inherent randomness. This stochastic nature of wind speed data can be effectively modeled using a Weibull distribution [35]. Accordingly, the probability density function of wind speed v is given as follows:

$$f(v; k_{wind}, \lambda_{wind}) = \frac{k_{wind}}{\lambda_{wind}} \left(\frac{v}{\lambda_{wind}} \right)^{k_{wind}-1} \exp \left[- \left(\frac{v}{\lambda_{wind}} \right)^{k_{wind}} \right] \quad (5)$$

where k_{wind} and λ_{wind} are the shape and scale parameters, respectively. To simulate the wind power, the wind speed data is substituted into the characteristic power function of the wind turbine [36]

$$P^{WT}(v(t), t) = \begin{cases} P_{rated}^W \times \frac{(v(t) - v_{ci})}{(v_{rated} - v_{ci})}, & v_{ci} \leq v(t) < v_{rated} \\ P_{rated}^W, & v_{rated} \leq v(t) < v_{co} \\ 0, & 0 \leq v(t) < v_{ci}, v_{co} < v(t) \end{cases} \quad (6)$$

where v_{ci} , v_{co} , and v_{rated} are the cut-in wind speed, cut-out wind speed and rated wind speed, respectively, and P_{rated}^W is the rated output power of WT.

There are many factors that affect the output power of PV, the main one being the intensity of solar radiation. The probability density function of solar radiation intensity r [37] is often expressed as a distribution

$$f(r; \alpha_{PV}, \beta_{PV}) = \frac{\Gamma(\alpha_{PV} + \beta_{PV})}{\Gamma(\alpha_{PV}) + \Gamma(\beta_{PV})} \left(\frac{r}{r_{max}} \right)^{\alpha_{PV}-1} \left(1 - \frac{r}{r_{max}} \right)^{\beta_{PV}-1} \quad (7)$$

where α_{PV} and β_{PV} are the parameters of the beta distribution, respectively; r_{max} is the maximum solar intensity, W/m^2 ; and Γ is the gamma function. In general, PV panels are often installed in places with abundant light resources, so the following formula is used to calculate the PV output power:

$$P^{PV}(r(t), t) = \begin{cases} \frac{\alpha_r}{K_r} \times Ar \times r^2, & r < K_r \\ \alpha_r \times Ar \times r, & r \geq K_r \end{cases} \quad (8)$$

where, A is the area of the solar panel, and $0.1 \leq \alpha_r \leq 0.2$, K_r is the threshold of solar radiation intensity.

In order to increase the utilization of renewable energy sources, ESS is used to store the power generated from renewable energy sources and increase the reliability of MG. Its charging and discharging process is modeled

$$SOC(t) = (1 - \tau)SOC(t-1) + \frac{P_{ESSc}(t)\Delta t\delta_c}{E_{ESS}^{\max}}F_{ESSc}(t) - \frac{P_{ESSd}(t)\Delta t}{E_{ESS}^{\max}\delta_d}F_{ESSd}(t) \quad (9)$$

$$\begin{cases} F_{ESSc}(t) = 1, F_{ESSd}(t) = 0, & ESS \text{ is charge} \\ F_{ESSc}(t) = 0, F_{ESSd}(t) = 1, & ESS \text{ is discharge} \\ F_{ESSc}(t) \cdot F_{ESSd}(t) = 0 \end{cases} \quad (10)$$

where $SOC(t)$ is the charge of the ESS under simulation at time t ; τ is the intrinsic discharge rate; $P_{ESSc}(t)$ and $P_{ESSd}(t)$ are the charge and discharge power of the ESS at simulation step t ; E_{ESS}^{\max} is the energy capacity value of the ESS; F_{ESSc} and F_{ESSd} are the charge and discharge state variables, respectively; δ_c and δ_d are the charge and discharge power efficiencies, respectively.

To ensure a reliable power supply in MGs with islanded operation capability, it is crucial to integrate dispatchable power sources, such as DE, as primary or backup reserves. However, diesel generators experience reduced efficiency under low load conditions, leading to higher

operational costs and accelerated component wear. To optimize the trade-off between reliability and economic performance [16], the generator's output must comply with the following constraints:

$$P_{DE}^{\min} \leq P_{DE}(t) \leq P_{DE}^{\max} \quad (11)$$

where P_{DE}^{\min} and P_{DE}^{\max} are the minimum and maximum output power of DE, respectively.

2.1.3. Energy dispatch model

Under the influence of earthquake, MGs will exist in the following three modes of operation: islanding operation (IO), joint operation (JO), and shutdown operation (SO). In the IO mode, the MGCC only considers the internal scheduling operation, and there is no power interaction with the rest of the MGs. In JO mode of MGs, there is an energy interaction that follows the rule of satisfying the excess energy interaction of the internal load demand first. In the SO mode, all the internal power equipment stops operating.

In the event of a fault, the primary operational objective of CPMMGs is to ensure a reliable power supply to users. Whether the MG operates in islanded mode or joint mode, the internal load demand must be prioritized. Consequently, the operational objectives of the MGCC remain consistent for both islanded and joint MGs, as below

$$\text{MinimiseOF}(t) = \sum_{m=1}^{N_{l,m}} a_{l,m} \varphi_{i,l,m}^C(t) LS_{l,m}(t), i \in V_C, l \in L_m, m \in (M_{JO} \cup M_{IO}) \quad (12)$$

where M_{JO} and M_{IO} are sets of MGs operating in JO mode and IO mode within CPMMGs, respectively; L_m denotes the set of users load in the m -th MG; l is the load labeling; $N_{l,m}$ is the load number in the m -th MG; $a_{l,m}$ is the importance of the load in the m -th MG; $LS_{l,m}(t)$ is the l -th user load to be curtailed in the m -th MG; $\varphi_{i,l,m}^C$ denotes the operational state of cyber node i , which is linked to the load of the l -th user in the m -th MG.

In addition to the model of DGs and the operational objectives of the MG, the constraints of CPMMGs must also be satisfied. These constraints include power balance equations, renewable energy power limits, DE power output limits, ESS charging and discharging constraints, and load curtailment limits. The mathematical formulations of these constraints are provided below, as follows:

Power balance constraints:

$$P_{WT,m}(t) + P_{PV,m}(t) + P_{ESSd,m}(t) - P_{ESSc,m}(t) + \sum_{d \in DE_m} P_{DE,m,d}(t) + P_m^{ex}(t) = L_m^{tot}(t) - \sum_{l \in N_{l,m}} \varphi_{i,l,m}^C(t) LS_{l,m}(t) \quad (13)$$

where DE_m denotes the set of DE in the m -th MG; $P_m^{ex}(t)$ represents the power exchange between MGs; L_m^{tot} is all the load demands in the MG. If MG operates in IO mode, $P_m^{ex}(t) = 0$. If MG operates in JO mode, $P_m^{ex}(t) \neq 0$.

Power constraints for renewable energy operation:

$$0 \leq P_{WT,m}(t) \leq \varphi_{i,WT,m}^C(t) \cdot P_{WT,m}^{\max}(t) \quad (14)$$

$$0 \leq P_{PV,m}(t) \leq \varphi_{i,PV,m}^C(t) \cdot P_{PV,m}^{\max}(t) \quad (15)$$

Power constraints for diesel generator operation:

$$\varphi_{i,dej,m}^C(t) \cdot P_{DE,m,d}^{\min} \leq P_{DE,m,d}(t) \leq \varphi_{i,dej,m}^C(t) \cdot P_{DE,m,d}^{\max}, \forall d \in DE_m \quad (16)$$

Power constraints on the operation of energy storage devices:

$$0 \leq P_{ESSc,m}(t) \leq \varphi_{i,ess,m}^C(t) \cdot P_{ESSc,m}^{\max} \quad (17)$$

$$0 \leq P_{ESSd,m}(t) \leq \varphi_{i,ess,m}^C(t) \cdot P_{ESSd,m}^{\max} \quad (18)$$

$$SOC_{\min} \leq SOC(t) \leq SOC_{\max} \quad (19)$$

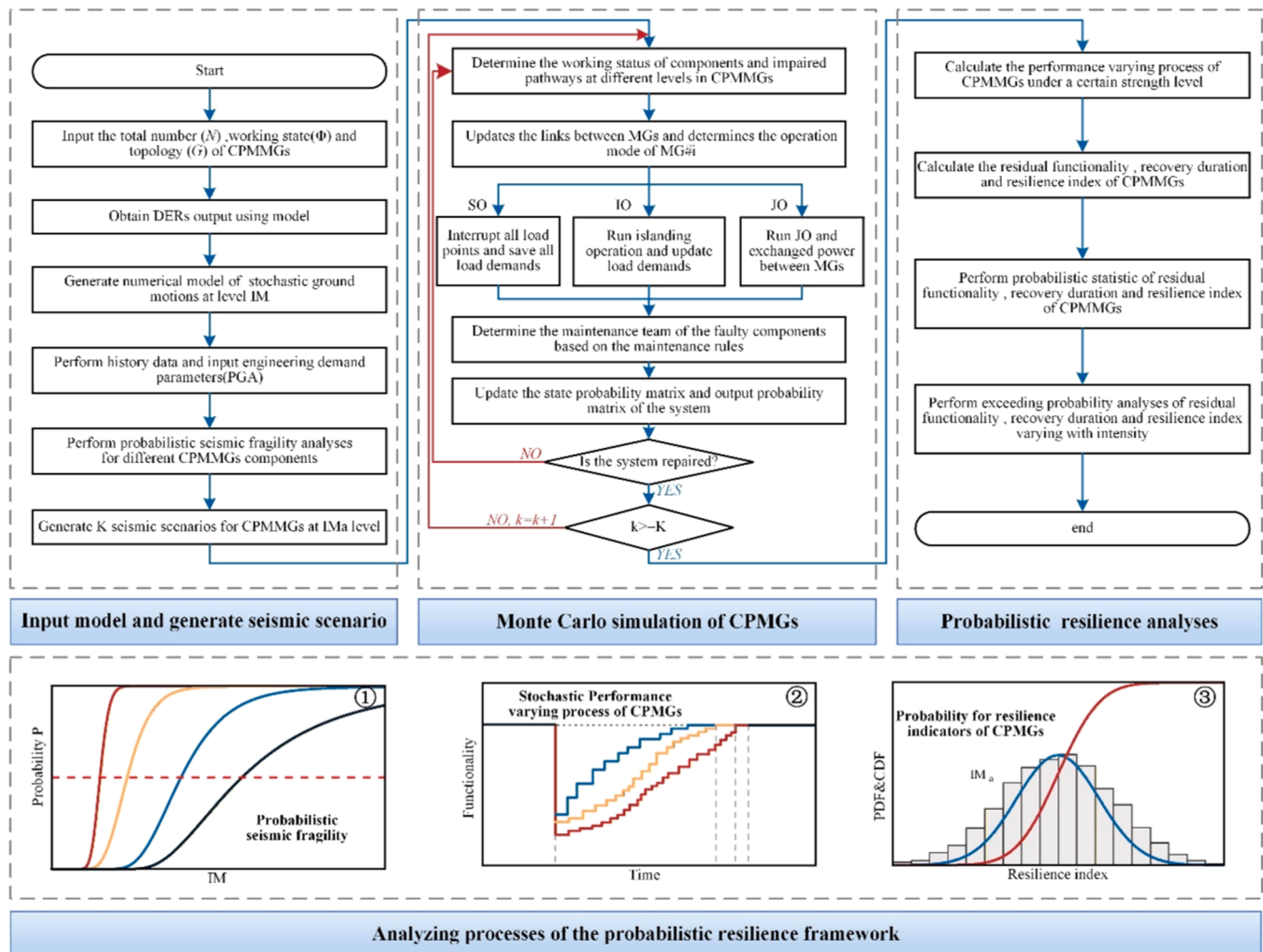


Fig. 2. Probabilistic seismic resilience assessment and analysis framework.

Power constraints for load shedding:

$$0 \leq LS_{l,m}(t) \leq L_{l,m}(t) \quad (20)$$

where $L_{l,m}$ denotes load demand of the l -th user in the m -th MG.

When MGs operate joint mode within CPMMGs, power interactions occur between them, resulting in a non-zero internal power value $P_m^{ex}(t)$ within each MG. If the DGs within a MG satisfy the load demand and energy storage requirements, the surplus power available for exchange is denoted as $P_m^{out,ex}(t) = P_m^{ex}(t) < 0$. Conversely, if there is a power deficit, it is represented as $P_m^{in,ex}(t) = P_m^{ex}(t) > 0$. $P_m^{shot}(t)$ and $P_m^{excess}(t)$ represent the power deficit and surplus of the MGs, respectively, and are transmitted from the MGCC to the CEMS. Based on this, the power distribution in the CEMS is determined as follows

$$P_m^{in,ex}(t) = \frac{P_m^{shot}(t) \sum_{m=1}^{N_{JO}} P_m^{excess}(t)}{\sum_{m=1}^{N_{JO}} P_m^{shot}(t)}, m \in M_{JO} \quad (21)$$

where N_{JO} is the number of MG operating in JO

2.2. Seismic damage modelling

Seismic index parameters are critical for evaluating the seismic resilience of CPMMGs. In engineering practice, key metrics such as peak ground acceleration (PGA) and spectral acceleration (SA) are widely employed to quantify seismic intensity. As demonstrated in the literature [21] and [38], PGA proves particularly suitable for rigid

infrastructure systems, such as transmission towers and substations, due to its direct correlation with structural loads in seismic scenarios.

Given the geographically dispersed configuration of CPMMGs, seismic wave attenuation effects must be rigorously addressed. Building upon seismic attenuation theory [39], the relationship between PGA and epicentral distance follows:

$$\ln \text{PGA} = F_1 + F_2 \cdot IM - F_3 \ln(D + 25) \quad (22)$$

where IM is Richter magnitude scale; D is epicentral distance; F_1 , F_2 , and F_3 are constants -0.152 , 0.859 , and -1.803 respectively.

A probabilistic seismic hazard model is constructed for urban-scale CPMMGs with a service radius of 80 km. Assuming uniform spatial distribution of potential epicenters within the circular domain [40], the probability density function of earthquake occurrence is defined as

$$f_D(d) = \begin{cases} \frac{2d}{R^2}, & 0 \leq d \leq R \\ 0, & \text{otherwise} \end{cases} \quad (23)$$

Fragility curves are widely adopted in seismic engineering to quantify the vulnerability of electrical components. As validated in prior studies [41], these curves are derived from lognormal probability distributions, where the mean value μ_e characterises the median structural resistance and the standard deviation σ_e reflects the degree of dispersion.

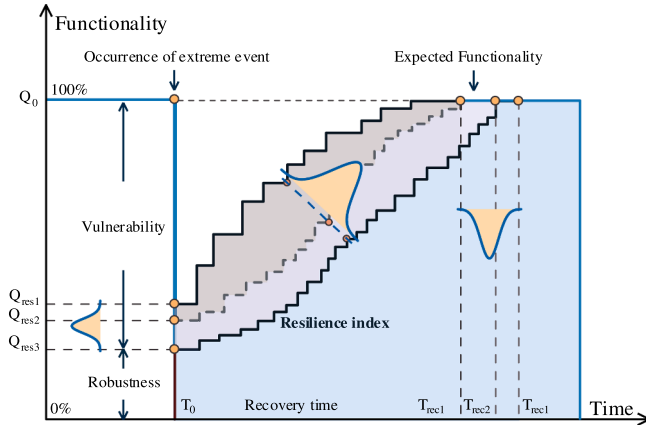


Fig. 3. Schematic view of system function.

$$P_e(PGA) = \Phi\left(\frac{\ln PGA - \mu_e}{\sigma_e}\right) \quad (24)$$

By incorporating site-specific PGA measurements, the component failure probability can be computed.

2.3. Modeling of restoration process

The post-earthquake resilience of CPMMGs serves as a critical indicator of their resilience engineering performance. Drawing on the repair dynamics model proposed in Ref. [42] and Ref. [43], this study assumes ideal conditions that disregard traffic network congestion and spare parts supply chain uncertainties. Under these assumptions, component repair times are modeled as following a two-parameter lognormal distribution:

$$f(t_e; \mu_{t_e}, \sigma_{t_e}) = \frac{1}{t_e \sigma_{t_e} \sqrt{2\pi}} \exp\left[-\left(\ln t_e - \mu_{t_e}\right)^2 / 2\sigma_{t_e}^2\right], t_e > 0 \quad (25)$$

where μ_{t_e} is mean of repair time and characterizes median repair duration, σ_{t_e} is standard deviation and accounts for uncertainties such as workforce skill variability.

Based on the autonomous nature of CPMMG, this study assumes that each MG contains independent cyber and physical maintenance units, and maintenance resources are not shared between MGs. The single-MG recovery time as

$$T_{MG_m} = \max\left(\sum_{i=1}^{N_{e,damage}^C} t_{e_i}^C, \sum_{j=1}^{N_{e,damage}^P} t_{e_j}^P\right) \quad (26)$$

where T_{MG_m} is recovery durations for the m -th MG. The $N_{e,damage}^C$ and $N_{e,damage}^P$ denote the number of damage node in the cyber system and physical system, respectively. Correspondingly, $t_{e_i}^C$ and $t_{e_j}^P$ indicate the repair time for component in the cyber system the physical system, respectively.

The complete restoration of CPMMGs is strictly defined as the state where all fault components regain operational functionality. Consequently, the total system recovery duration

$$T_S = \max\{T_{MG_m}, m \in M\} \quad (27)$$

where T_S is recovery time of CPMMGs, M denotes the set of all MGs in the CPMMGs.

3. Seismic resilience assessment and analysis

3.1. Probabilistic resilience assessment and analysis framework

Fig. 2 presents the probabilistic seismic resilience assessment

Table 1

Capacity of distributed generation in each of the MGs.

Parameter	Unit	#	MG#1	MG#2	MG#3	MG#4	MG#5
P_{WT}^{rated}	MW	-	0.5	1.1	0.8	1	0.6
P_{PV}^{rated}	MW	-	1.2	0.5	0.8	0.6	1
$P_{ESS}^{max}, P_{ESSd}^{max}$	MW	-	0.4	0.3	0.3	0.3	0.4
γ_c, γ_d	MW	-	0.9	0.9	0.9	0.9	0.9
F_{max}^{ESS}	MW	-	1.2	0.8	0.8	0.8	1
P_{DE}^{max}	MW	1	0.4	0.3	0.3	0.5	0.4
P_{DE}^{max}	MW	2	0.3	0.5	-	0.5	0.4

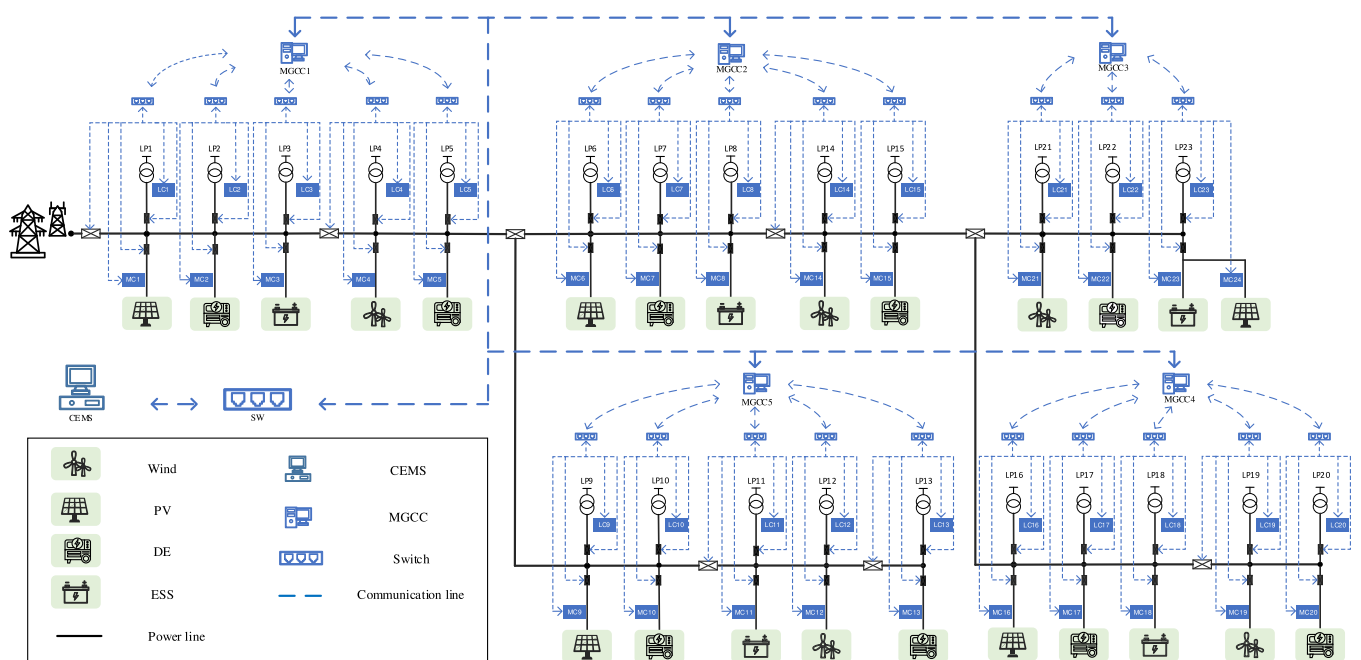


Fig. 4. CPMMG architecture.

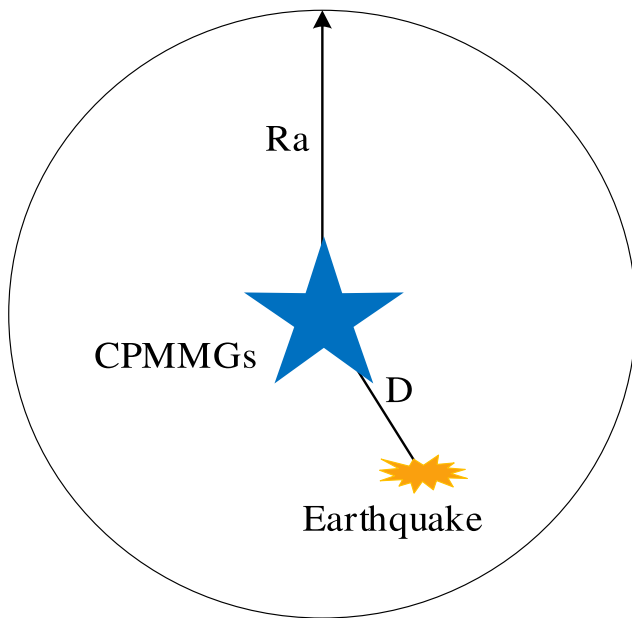


Fig. 5. Earthquake simulation.

Table 2

Standard deviation and mean values of the fragility curves for different components.

Equipment	σ_e	μ_e
DG	0.5	0.48
Transformer	0.7	0.75
Circuit Breaker	0.47	0.65
Disconnector Switch	0.7	1.2
Line	0.5	1.2
Controller	0.7	1.2

Table 3

Standard deviation and mean values of the repair time for different components.

Equipment	σ_{t_e}	μ_{t_e}
DG	5.3	8
Transformer	5.07	8
Circuit Breaker	1.67	5
Disconnector Switch	2.78	5.9
Line	2.7	4
Controller	5.2	12

framework and simulation flowchart developed in this study. The framework comprises three key components: (1) input parameter configuration and hazard scenario generation, (2) Monte Carlo simulation of CPMMGs, and (3) probabilistic resilience quantification. In the initial phase, model parameters and simulation iterations are configured, followed by the determination of seismic intensity levels, affected geographical regions, and component damage probability functions. The subsequent phase involves three critical operations: a) damage state evaluation for individual components, b) operational mode analysis considering damage propagation paths, and c) energy dispatch optimization with repair process simulation. This phase generates topological functionality matrices and operational performance matrices. In the final analysis phase, the variation in system functionality is used to describe the stochastic residual system capacity over time under specific seismic intensities. Through statistical analysis, this phase establishes probability models for three key metrics: residual functionality, recovery duration, and resilience index. Subsequently, exceedance

probability analysis is conducted for target resilience thresholds across multiple intensity levels, completing the probabilistic resilience assessment. Section II comprehensively explains the Monte Carlo simulation process for CPMMGs in the first two phases of the probabilistic assessment framework. The following subsections will provide a detailed explanation of the system functionality modeling approach and the probabilistic resilience metrics.

3.2. System functionality

CPMMGs prioritize load energy supply as their operational objective, with system performance quantified through two key metrics: power delivery rate and power supply reliability rate. The power transmission rate characterizes the impact of network topology on power delivery efficiency, while the power supply reliability rate evaluates the effectiveness of DGs power output and power dispatch strategies.

In CPMMGs, power delivery paths and information transmission paths together constitute the dual infrastructure framework underpinning system operation. A power delivery path is defined as a continuous electrical connection linking DGs nodes to load nodes within permissible operational constraints. An information path represents a reliable communication channel connecting controller nodes to terminal devices. In practical implementations, the synergistic constraints resulting from this cyber–physical coupling do not influence power transmission through a simple linear superposition. Accordingly, the power delivery rate η_{Tr} can be mathematically expressed as

$$\eta_{Tr} = \sqrt{\eta_{Tr}^P \cdot \eta_{Tr}^C} \quad (28)$$

where η_{Tr}^P is the residual power path ratio post-earthquake in the physical system, η_{Tr}^C is the residual information transmission ratio post-earthquake in the cyber system.

The power supply reliability rate η_s serves as a critical indicator for evaluating the output performance of CPMMGs. A higher η_s directly correlates with enhanced operational reliability of both DGs and the power dispatch system within the CPMMGs. Mathematically expressed as

$$\eta_s = \frac{P_{\text{supplied}}}{P_{\text{demand}}} \quad (29)$$

where, P_{supplied} is the actual supplied power in the CPMMGs; P_{demand} is the power demand of users in the CPMMGs.

This study proposes a weighted composite index integrating power delivery rate η_{Tr} and power supply reliability rate η_s to evaluate the functional state of CPMMGs under post-earthquake conditions. To address the dynamic coupling between topological resilience and output efficacy in heterogeneous architectures, we introduce a weighting coefficient $\omega \in [0, 1]$, yielding the system functionality

$$Q = \omega \cdot \eta_{Tr} + (1 - \omega) \cdot \eta_s \quad (30)$$

The system functionality of CPMMGs is a quantifiable measure of overall performance, derived from the structural integrity of the physical infrastructure and the reliability of the power supply. The latter directly reflects the effectiveness of scheduling strategies and the output of DGs. A weighting factor ω is applied to balance the emphasis between structural Vulnerability and operational reliability, allowing the metric to simultaneously capture the system's inherent disaster resistance and its operational adaptability during extreme events.

3.3. Probabilistic resilience index

Under seismic disturbances of specific magnitudes, the functionality evolution of CPMMGs is illustrated in Fig. 3. At the earthquake initiation instant T_0 , the system functionality Q_{IM} plummets to Q_{res} . As faulty components are progressively restored following the repair sequence,

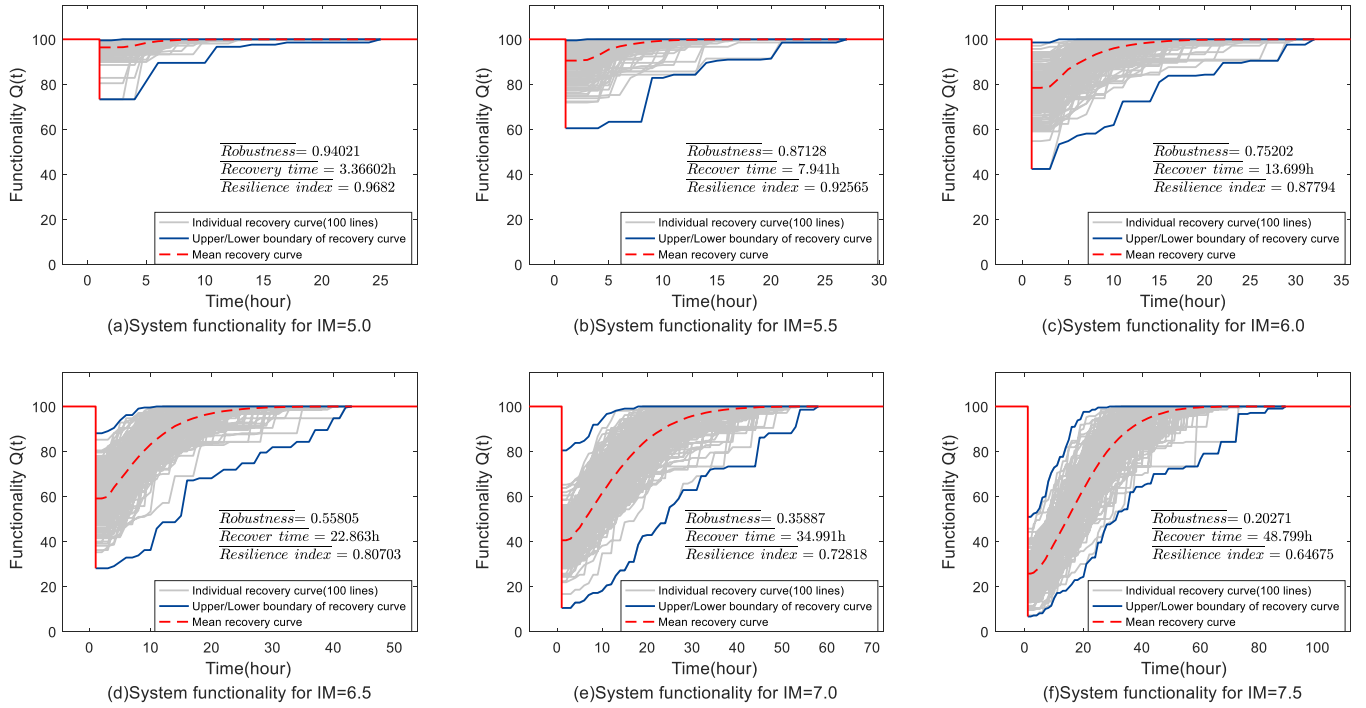


Fig. 6. System functionality changes of CPMMGs for different earthquake intensities.

Table 4
 Standard deviation and mean values of the repair time for different components.

Earthquake intensity	Mean robustness index	Mean recovery time (hour)	Mean resilience index
5.0	0.9402	3.3660	0.9648
5.5	0.8713	7.9410	0.9157
6.0	0.7520	13.6990	0.8627
6.5	0.5581	22.8630	0.7891
7.0	0.3589	34.9910	0.7112
7.5	0.2027	48.7990	0.6331
8.0	0.1011	65.344	0.5818

system functionality exhibits stepwise recovery. This study focuses on assessing the inherent seismic resilience of CPMMGs, explicitly excluding external interventions such as equipment upgrades, thereby ensuring restoration to the pre-seismic baseline state Q_0 .

The post-seismic system robustness R_r can be quantified by the residual functionality Q_{res} , with the recovery duration defined as $R_r = T_{rec} - T_0$, as illustrated in Fig. 3. Building upon the resilience quantification framework proposed in [35], the seismic resilience index R_{IM} is defined as:

$$R_{IM} = \int_{T_0}^{T_{rec}} Q_{IM}(t) / (T_{rec} - T_0) \cdot dt \quad (31)$$

where $R_{IM} \in [0, 1]$. A value of $R_{IM} = 0$ indicates complete system instability with no self-healing capacity, while $R_{IM} = 1$ signifies ideal disturbance immunity.

The stochastic nature of seismic events introduces inherent randomness in system resilience, transforming deterministic single-event assessments into probabilistic evaluations. For probabilistic resilience analysis, exceedance probabilities of resilience indices across varying seismic intensity levels can be quantified using maximum likelihood estimation [44]. Resilience index follow a truncated weibull distribution [45], the exceedance probability $P_R(x)$ is defined as:

$$P_R(x) = P(R_{IM} > R_{IM}^{tar} | IM = x) = 1 - \frac{1 - \exp\left[-\left(\frac{R_{IM}^{tar}}{\lambda_{R|IM}}\right)^{k_{R|IM}}\right]}{1 - \exp\left[-\left(\frac{1}{\lambda_{R|IM}}\right)^{k_{R|IM}}\right]}, \quad 0 \leq R_{IM}^{tar} \leq 1 \quad (32)$$

where R_{IM}^{tar} denotes the target resilience index. $k_{R|IM}$ and $\lambda_{R|IM}$ are the shape parameter and scale parameter of the truncated Weibull distribution for the resilience index. $k_{R|IM}$ can be obtained by maximum likelihood estimation. Besides, $\lambda_{R|IM}$ can be derived using Eq. (33):

$$\ln\lambda_{R|IM} = \theta_0 + \theta_1 \cdot \ln IM \quad (33)$$

where θ_0 and θ_1 are regression parameters for resilience exceedance probability. Subsequently, the probabilistic seismic hazard data, denoted as $\mathcal{V}(IM > x)$ [44], representing the annual probability of exceeding a certain intensity level at the target site, is incorporated into the analysis. By convolving this hazard data with the conditional probability of exceeding a specified resilience index $P(R_{IM} > R_{IM}^{tar} | IM = x)$, one can obtain the annual exceedance probability of the resilience index $\mathcal{V}(R_{IM} > R_{IM}^{tar})$. The detailed calculation procedure is expressed explicitly in Eq. (34).

$$\mathcal{V}(R_{IM} > R_{IM}^{tar}) = \int_0^{\infty} P(R_{IM} > R_{IM}^{tar} | IM = x) \cdot d\mathcal{V}(IM > x) \quad (34)$$

Furthermore, based on the assumption of a Poisson stochastic process, the life-cycle exceedance probability of the resilience index over a service period of y years, denoted as $\nu_{y-year}(R_{IM} > R_{IM}^{tar})$, can be derived accordingly. The mathematical formulation of this probability is explicitly provided in Eq. (35).

$$\mathcal{V}_{y-year}(R_{IM} > R_{IM}^{tar}) = 1 - \exp[-y \cdot \mathcal{V}(R_{IM} > R_{IM}^{tar})] \quad (35)$$

where y denotes the number of years considered in the service life-cycle.

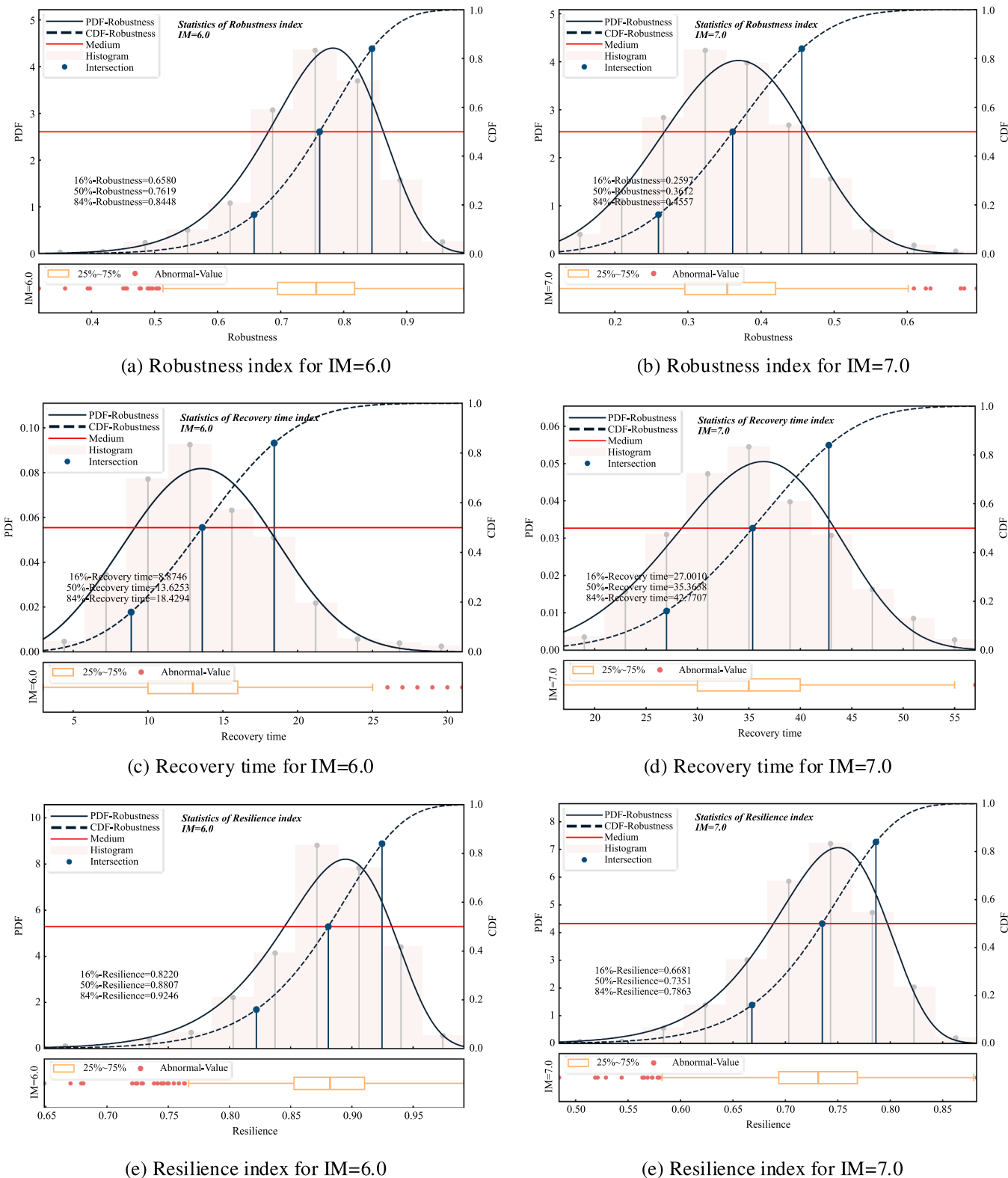


Fig. 7. Probabilistic statistics of robustness index, recovery time and resilience index.

4. Case study

4.1. Input data

This study develops a CPMMGs based on the IEEE RBTS [46] reliability assessment framework. The system architecture, as shown in

Fig. 4, integrates five MGs into a Bus6 Feeder F4 distribution network through DG units, intelligent circuit breakers, and cyber-physical communication infrastructure referenced from [16]. Each MG incorporates renewable energy sources, such as wind and photovoltaic, energy storage systems, and diesel generators, with load characteristics following a normal distribution. Key system parameters are detailed in

Table 5

Quantiles in probabilistic statistics of robustness index, recovery time.

Performance index	Robustness index	Recovery time(hour)	Resilience index
16 % for IM = 5.0	0.8833	3.4691	0.89
50 % for IM = 5.0	0.9464	5.7232	0.9593
84 % for IM = 5.0	0.9936	8.1431	1.0000
16 % for IM = 5.5	0.8641	4.6251	0.8641
50 % for IM = 5.5	0.	8.0053	0.9258
84 % for IM = 5.5	0.9561	11.7819	0.9719
16 % for IM = 6.0	0.6580	8.874	0.8220
50 % for IM = 6.0	0.7619	12.6253	0.8807
84 % for IM = 6.0	0.8448	18.4294	0.9246
16 % for IM = 6.5	0.4507	16.3549	0.7526
50 % for IM = 6.5	0.5656	22.9835	0.8142
84 % for IM = 6.5	0.6637	29.2086	0.8605
16 % for IM = 7.0	0.2597	27.0010	0.6681
50 % for IM = 7.0	0.3612	35.3658	0.7351
84 % for IM = 7.0	0.4557	42.427707	0.7863
16 % for IM = 7.5	0.1280	38.6587	0.5826
50 % for IM = 7.5	0.2014	49.1851	0.6539
84 % for IM = 7.5	0.2771	58.2784	0.7093
16 % for IM = 8.0	0.0532	53.7049	0.5070
50 % for IM = 8.0	0.0974	65.9294	0.5799
84 % for IM = 8.0	0.1491	76.1764	0.6375

Table 1.

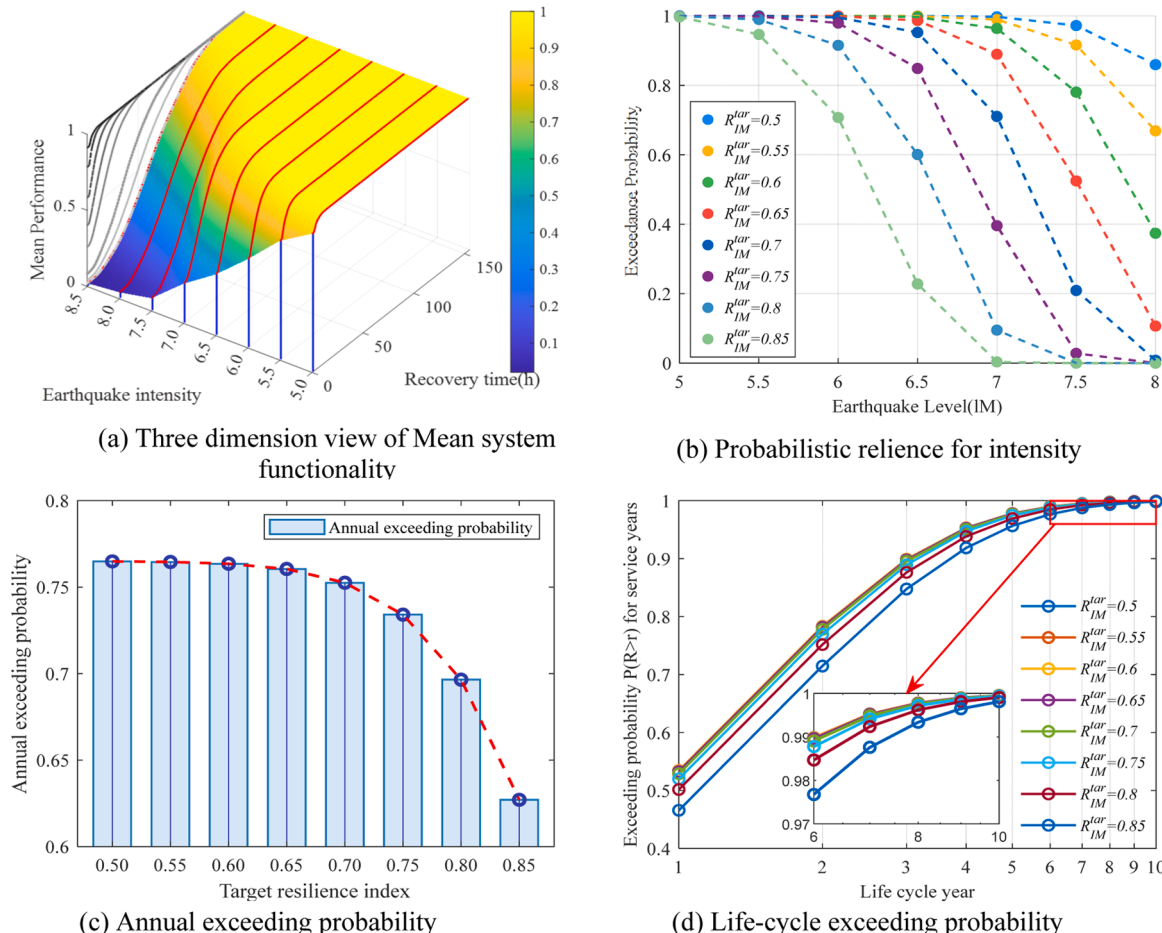
In the seismic vulnerability analysis, a city-scale impact radius of 80 km and earthquakes with magnitudes ranging from 5.0 to 8.0 were considered. The simulation scope is illustrated in Fig. 5. The PGA vulnerability parameters for the components of the CPMMGs are provided in Table 2 [21]. Maintenance operations adhere to the requirements of protection zoning, and each MG has independent

personnel for power and ICT system maintenance, eliminating the issue of cross-zone resource sharing. The log-normal distribution parameters for the component repair times of the CPMMGs are presented in Table 3 [42].

4.2. Result

The functionality response of CPMMGs under seismic events of varying intensities is illustrated in Fig. 6. The impact of earthquakes on system performance intensifies with the increase in seismic intensity. Due to the extensive coverage and large simulation area of CPMMGs, components of CPMMGs experience varying degrees of damage even under earthquakes of the same intensity. As shown in Figs. 6(c)–(e), the Monte Carlo simulation of system functionality Q exhibits a wide variation under seismic intensities of 5.5–7.0. In the CPMMGs topology, certain components with high connectivity can cause widespread component failure if damaged. Similarly, the failure of MGCC, which holds a high control level in the information system, can also lead to extensive component inoperability. When the seismic intensity reaches 7.5, the system functionality of CPMMGs shows a narrower range of variation due to the extensive damage scope.

Table 4 summarizes the evaluation metrics for system functionality of CPMMGs: robustness, recovery time, and resilience, under seismic events of varying intensities. As the seismic intensity increases from 5.0 to 7.5, the mean resilience of CPMMGs decreases from 0.9682 to 0.64675, while the average robustness shows a significant decline from 0.94021 to 0.20271. With higher seismic intensities, the failure scope of CPMMGs expands, leading to a gradual increase in the average recovery time of system functionality Q . As shown in Fig. 6(f), the maximum

**Fig. 8.** Probabilistic seismic system functionality and resilience index analysis.

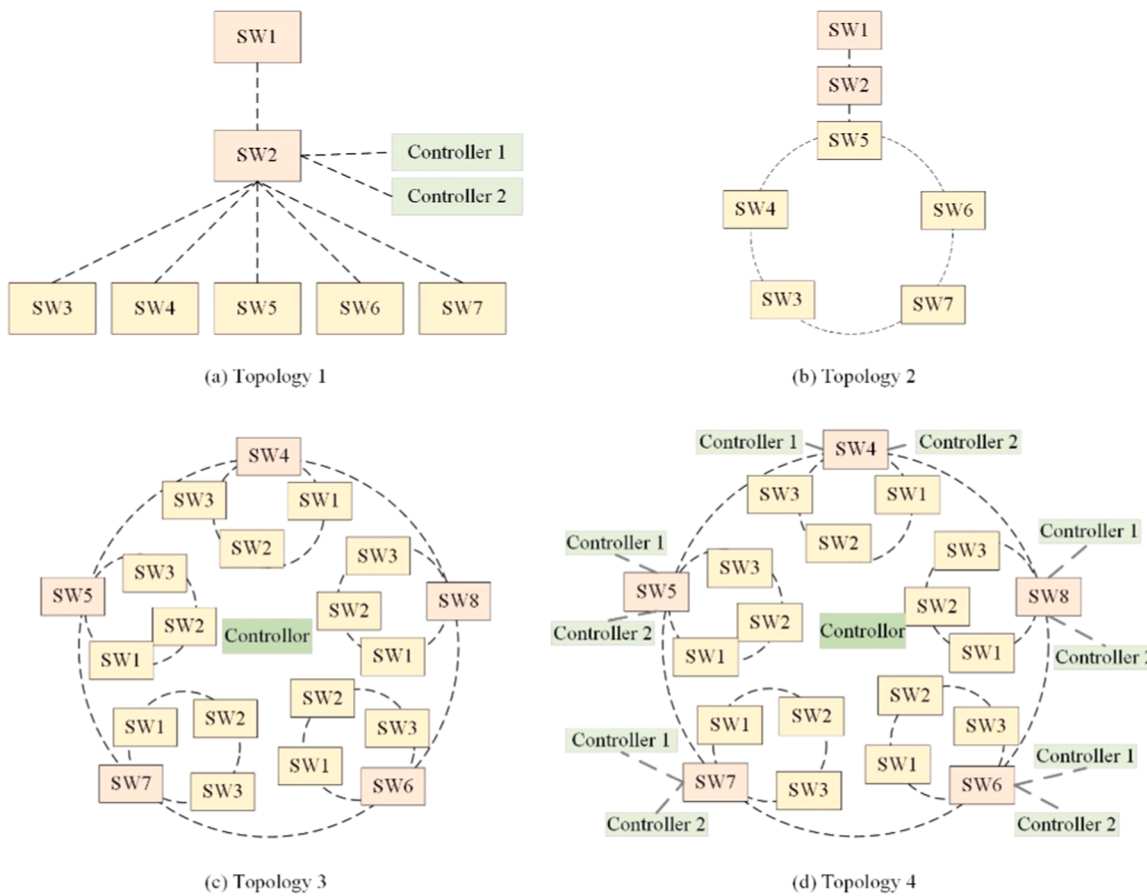


Fig. 9. Probabilistic seismic system functionality and resilience index.

recovery time can reach up to 90 h.

Seismic intensity 5.0 causes minimal damage to CPMMGs, while intensity 7.5 occurs less frequently. Therefore, this study focuses on seismic scenarios with intensities 5.5 and 6.5 to analyze the statistical properties of CPMMGs' system functionality metrics: robustness, recovery time, and resilience. Fig. 7 presents a statistical analysis of the truncated Weibull distribution and data dispersion of these metrics under seismic intensities 6.0 and 7.0. The statistical analysis of the probability characteristics for the remaining intensities is shown in Table 5. Due to the extensive coverage of CPMMGs and the varying importance of internal components to system operation, the three metrics exhibit a significant number of outliers.

Fig. 8 presents the probabilistic analysis results of CPMMGs' system functionality and resilience metrics. Fig. 8(a) clearly illustrates the changes in the mean system performance of CPMMGs. As the seismic intensity increases from 5.0 to 8.0, the recovery time of system functionality rises sharply, while system robustness gradually declines. Fig. 8(b) discusses the exceedance probability of the six-target resilience metrics within the range of 0.5–0.85. It is observed that the exceedance probabilities of all six resilience targets decrease rapidly when the seismic intensity exceeds 0.65, indicating a significant decline in the seismic resilience of the tested CPMMGs under such conditions. Figs. 8(c) and 8(d) analyze the seismic resilience probability of the CPMMGs system from different time scales. Fig. 8(c) focuses on the annual seismic risk, with the target probability ranging from 0.5 to 0.85, and the average annual exceedance probability between 0.65 and 0.78. It shows a decreasing trend, aligning with the rule that higher seismic intensity corresponds to lower occurrence probability. Fig. 8(d) presents the exceedance probability over a service life of 1 to 10 years. The exceedance probability increases cumulatively over time, though the growth rate may slow down. Additionally, under the same service year, a lower

target resilience index corresponds to a higher exceedance probability.

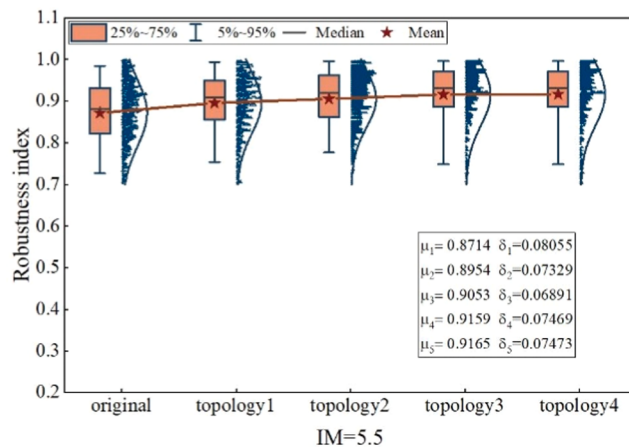
4.3. Discussion

The resilience of CPMMGs is governed by diverse factors, which this study categorizes into internal and external determinants. Internal factors pertain to the system's intrinsic properties, encompassing both the information and physical subsystems. Key examples include variations in information topology and the composition of distributed energy resources. External factors encompass post-disaster interventions, such as maintenance protocols implemented by support teams, which directly shape system recovery and performance.

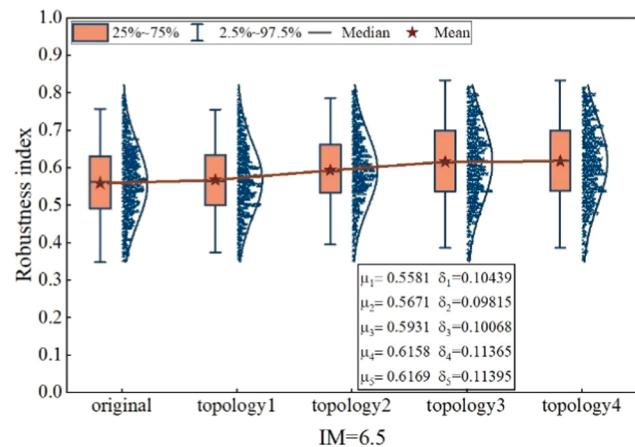
4.3.1. The impact of information network topology for resilience index

Due to the coupling relationship between the cyber system and the physical system of CPMMGs, it is meaningful to explore different information topologies for the resilience of CPMMGs. The information topology of CPMMGs can be categorized into the backbone network layer and the core network layer, with the backbone layer being the management layer of the MGs, and the core network layer being the layer of the power interactions between multiple MGs. The four evaluated topologies are illustrated in Fig. 9, each representing progressive enhancements to the original centralized communication architecture: (1) Topology 1 (Fig. 9(a)): Incorporates redundant controllers within the backbone layer. (2) Topology 2 (Fig. 9(b)): Introduces additional communication links in the backbone layer. (3) Topology 3 (Fig. 9(c)): Extends redundancy to both backbone and core layers through supplementary communication lines. (4) Topology 4 (Fig. 9(d)): Builds upon Topology 3 by integrating additional redundant controllers.

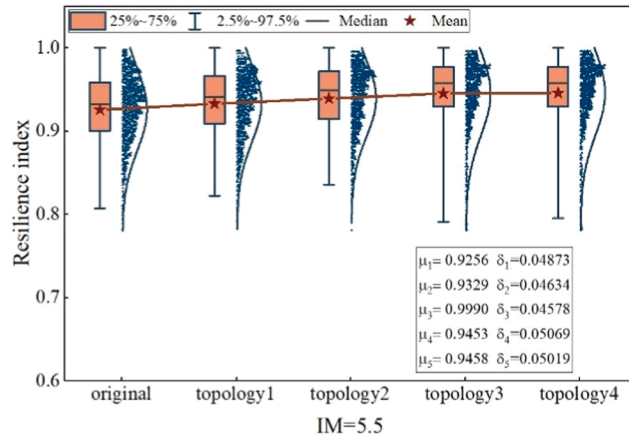
Fig. 10 compares variations in robustness and resilience metrics across different communication topologies under seismic intensities of



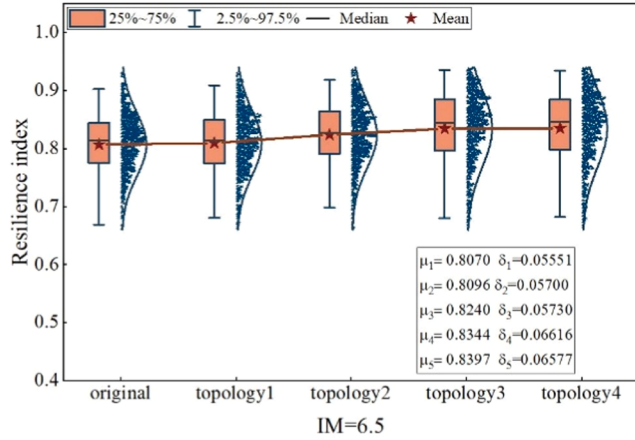
(a) Robustness indices of different topologies for IM=5.5



(b) Robustness indices of different topologies for IM=6.5



(c) Resilience indices of different topologies for IM=5.5



(d) Resilience indices of different topologies for IM=6.5

Fig. 10. Comparison of robustness index and resilience index of 4 topologies for IM = 5.5 and IM = 6.5.

5.5 and 6.5. The results demonstrate that modifications in Topologies 1–4 consistently improve both robustness and resilience metrics of CPMMGs. However, Topology 3 exhibits the most significant enhancement, with Topology 4 showing equivalent mean values to Topology 3. This indicates that expanding communication line redundancy in the network topology more effectively improves seismic resilience compared to implementing redundant controllers. Furthermore, comparative analysis of Topologies 2 and 3 reveals that backbone layer and core layer interconnectivity critically influences CPMMGs' resilience enhancement.

4.3.2. The impact of DGs configuration in MG for resilience index

This case study examines the impact of DGs configurations on resilience in CPMMGs. To evaluate how DGs allocations affect system performance, this study analyzes five MG configurations: MG1 retains its baseline setup; MG2 excludes PV; MG3 comprises only PV, ESS, and a DE; MG4 operates without ESS; and MG5 removes DEs entirely.

Fig. 11 demonstrates the impact of DGs reconfiguration on system functional robustness and resilience indices under seismic intensity levels 5.5 and 6.5. Under intensity 5.5 conditions, both robustness and resilience indices exhibited moderate declines post-reconfiguration. Notably, MG2 and MG3 showed greater reductions in average resilience indices compared to robustness metrics, 0.168 decrease in MG3, attributable to the absence of PV in MG2 and WT in MG3, which compromised power supply reliability. MG3's reliance solely on PV with integrated ESS further amplified this effect. Comparative analysis reveals that distributed DG deployment enhances seismic resilience. When

seismic intensity increased to level 8, a significant robustness deterioration was observed. The coordinated operation mode in CPMMGs precipitated a 0.180 decline in MG1's average resilience index. These findings confirm that optimized DG configuration with spatial dispersion and balanced capacity allocation significantly improves CPMMGs' seismic resilience, particularly when aligned with individual MG load requirements.

4.3.3. The impact of recovery strategies on resilience index

The scheduling of repair workforce constitutes a critical factor influencing the post-disaster recovery capability of CPMMGs. In industrial maintenance systems, queuing theory has been widely adopted to optimize repair scheduling and workforce allocation. Two prevalent operational paradigms in this context include stochastic repair strategy and shortest-wait-time strategy. The former approach randomly selects damaged components for repair, while the latter prioritizes elements based on their accumulated downtime since failure occurrence. These contrasting methodologies demonstrate fundamentally different optimization philosophies in maintenance operations management. **Table 6** presents a comparative analysis of two maintenance strategies in CPMMGs based on their average resilience indices. Under low seismic intensity conditions, both strategies exhibited negligible differences in resilience performance. However, as seismic intensity increased, the shortest-wait-time strategy demonstrated significantly superior resilience indices compared to the random repair approach. These results indicate that the shortest-wait-time strategy accelerates post-earthquake response times and enhances CPMMGs' seismic resilience by prioritizing

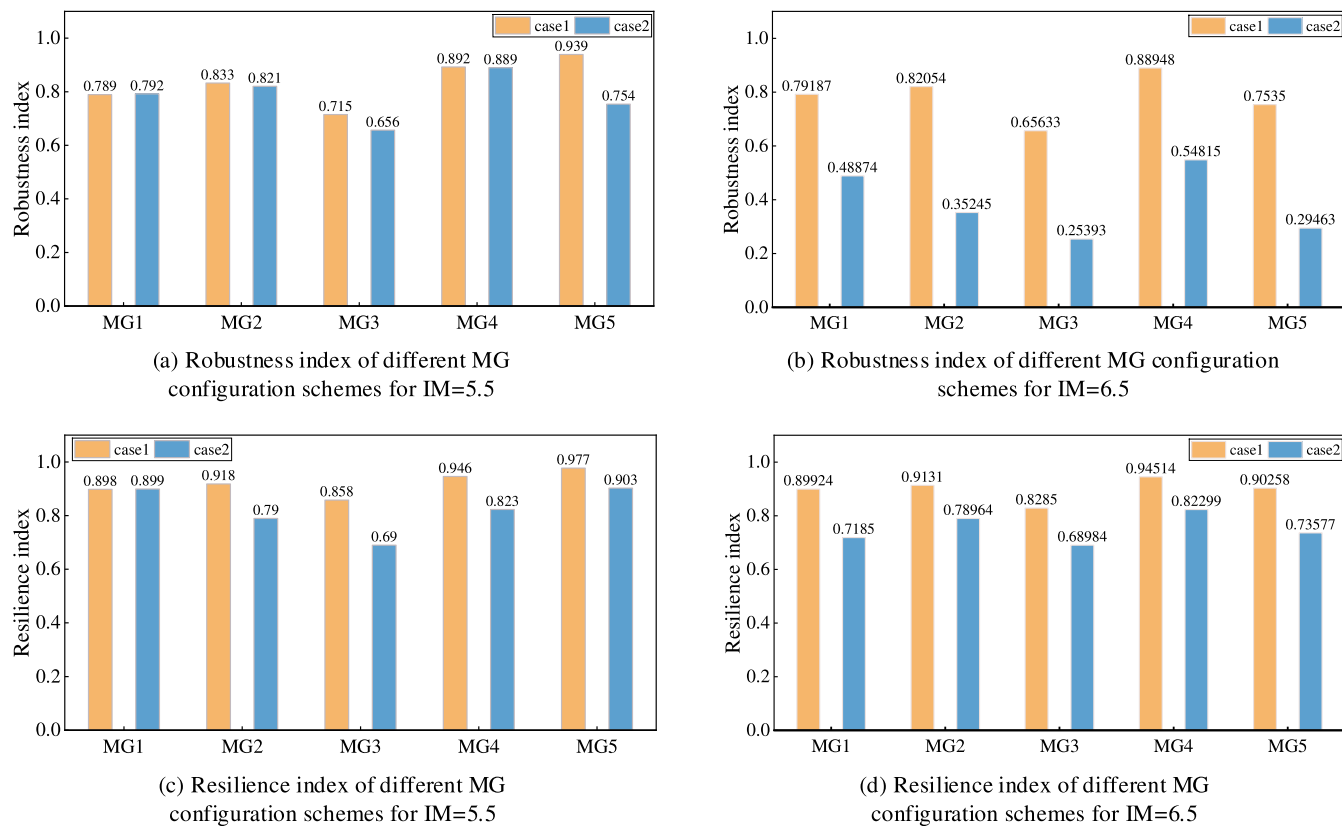


Fig. 11. Robustness index and resilience index comparison before and after configuration.

Table 6
Resilience index for two repair strategies.

Strategy	R _{IM} for IM = 5.0	R _{IM} for IM = 5.5	R _{IM} for IM = 6.0	R _{IM} for IM = 6.5	R _{IM} for IM = 7.0	R _{IM} for IM = 7.5
stochastic repair strategy	0.9648	0.9157	0.8627	0.7891	0.7112	0.6331
shortest-wait-time strategy	0.9682	0.9257	0.8780	0.8070	0.7282	0.6468

critical repairs systematically.

5. Conclusion

This study develops a probabilistic resilience assessment framework for CPMMGs, addressing critical challenges in evaluating seismic resilience of centralized architectures. Through experimental validation using improved CPMMGs based on IEEE RBTS, we demonstrate three main contributions: (1) Characterization of cross-domain fault propagation mechanisms in CPMMGs topologies; (2) Development of seismic damage modeling incorporating three post-disaster operational modes; (3) Formulation of a composite resilience metric integrating power transmission efficiency and supply reliability. The framework's innovation manifests in three aspects: first, through dual modeling of topological configuration and operational dynamics that enhance system functionality; second, the probabilistic resilience assessment framework systematically considers the uncertainty of earthquakes and the variability of renewable energy sources; and finally, an integrated system function that incorporates power delivery rate and power supply reliability rated is proposed, which is able to effectively reflect the attributes of CPMMGs. Case studies and comparisons are presented to provide a basis for disaster resilience planning for CPMMGs.

Current limitations involve three key assumptions: inherent stochasticity in Monte Carlo simulations, unmodeled interactions in DG configuration experiments, and idealized communication protocols

without considering network congestion. These simplifications potentially influence cross-domain fault propagation and post-seismic resilience dynamics. Future research directions will prioritize resource-constrained recovery optimization, particularly investigating optimal resilience enhancement strategies under finite repair resources and realistic communication constraints.

CRediT authorship contribution statement

Qiaoyuan Kou: Writing – original draft, Methodology, Data curation. **Hongli Zhang:** Writing – review & editing, Supervision, Conceptualization. **Cong Wang:** Software, Investigation. **Yue Meng:** Visualization, Validation.

Declaration of competing interest

The authors declare that they have no known competing financial interests or personal relationships that could have appeared to influence the work reported in this paper.

Acknowledgements

This work was supported by the National Natural Science Foundation of China (Grant Nos. 52267010, 52567014, 52565062), the Tianshan Talent Training Program (Grant Nos. 2023TSYCCX0037,

2023TSYCQNTJ0020, 2024TSYCLJ0008), and the Tianshan Innovative Research Team (Grant No. 2025D14009).

Data availability

Data will be made available on request.

References

- [1] Backhaus SN, Dobriansky L, Glover S, Liu C-C, Looney P, Mashayekh S, et al. Networked microgrids scoping study. 2016.
- [2] Zhou B, Zou J, Yung Chung C, Wang H, Liu N, Voropai N, et al. Multi-microgrid Energy Management systems: architecture, communication, and scheduling strategies. *J Mod Power Syst Clean Energy* 2021;9:463–76.
- [3] Kazama M, Noda T. Damage statistics (Summary of the 2011 off the Pacific Coast of Tohoku Earthquake damage). *Soils Found* 2012;52:780–92.
- [4] Jufri FH, Widiputra V, Jung J. State-of-the-art review on power grid resilience to extreme weather events: definitions, frameworks, quantitative assessment methodologies, and enhancement strategies. *Appl Energy* 2019;239:1049–65.
- [5] Dileep G. A survey on smart grid technologies and applications. *Renew Energy* 2020;146:2589–625.
- [6] Vu TV, Nguyen BLH, Cheng Z, Chow M-Y, Zhang B. Cyber-physical microgrids: toward future resilient communities. *IEEE Ind Electron Mag* 2020;14:4–17.
- [7] Badr A, Li Z, El-Dakhakhni W. Probabilistic dynamic resilience quantification for infrastructure systems in multi-hazard environments. *Int J Crit Infrastruct Prot* 2024;46:100698.
- [8] Cao X-Y, Feng D-C. Probabilistic resilience assessment of structures considering the functional uncertainty: a case study for external prestressed subframe in strengthening. *Eng Struct* 2025;332:119968.
- [9] Zhao Z, Xie J, Xu J, Xi L, Gong S, Lu J, et al. Assessment and mitigation of multi-mode oscillations in wind-solar hybrid multi-microgrids. *IEEE Trans Smart Grid* 2024;15:1330–45.
- [10] Wang Y, Qiu D, Wang Y, Sun M, Strbac G. Graph learning-based voltage regulation in distribution networks with multi-microgrids. *IEEE Trans Power Syst* 2024;39: 1881–95.
- [11] Mansouri M, Eskandari M, Asadi Y, Savkin A. A cloud-fog computing framework for real-time energy management in multi-microgrid system utilizing deep reinforcement learning. *J Energy Storage* 2024;97:112912.
- [12] Mumtaz F, Imran K, Rehman H, Bukhari SBA. Novel protection method for AC microgrids with multiple distributed generations using unscented Kalman filter. *Electr Power Syst Res* 2024;230:110227.
- [13] Shaker HK, Mahmoud I, Mosa MA, Abdel-Latif KM, Ali AA, Keshta HE. Optimal dual control strategy for multi-interconnected microgrids under unintentional islanding and fault scenarios. *IEEE Access* 2025;13:82680–97.
- [14] Ward L, Subbaraj A, Demir A, Chamana M, Bayne SB. Analysis of grid-forming inverter controls for grid-connected and islanded microgrid integration. *Sustainability* 2024;16:2148.
- [15] Wang C, Zhang T, Luo F, Li F, Liu Y. Impacts of cyber system on microgrid operational reliability. *IEEE Trans Smart Grid* 2019;10:105–15.
- [16] Barani M, Vadlamudi VV, Farzin H. Impact of cyber failures on operation and adequacy of Multi-Microgrid distribution systems. *Appl Energy* 2023;348:121437.
- [17] Xiao J, Wang L, Shafee Q, Bauer P, Qin Z. Cyber resilient communication network design for secondary control of microgrids. *IEEE Trans Ind Inform* 2025;21: 6071–80.
- [18] Ti B, Li G, Zhou M, Wang J. Resilience assessment and improvement for cyber-physical power systems under typhoon disasters. *IEEE Trans Smart Grid* 2022;13: 783–94.
- [19] Gautam P, Piya P, Karki R. Resilience assessment of distribution systems integrated with distributed energy resources. *IEEE Trans Sustain Energy* 2021;12:338–48.
- [20] Ferrario E, Poulos A, Castro S, De La, Llera JC, Lorca A. Predictive capacity of topological measures in evaluating seismic risk and resilience of electric power networks. *Reliab Eng Syst Saf* 2022;217:108040.
- [21] Amani-Jouneghani F, Fotuhi-Firuzabad M, Moeini-Aghaie M, Dehghanian P. Seismic resilience assessment of electric power distribution networks. *IEEE Trans Power Deliv* 2025;40:387–97.
- [22] Zhang W, Han Q, Shang W-L, Xu C. Seismic resilience assessment of interdependent urban transportation-electric power system under uncertainty. *Transp Res Part Policy Pract* 2024;183:104078.
- [23] Farzin H, Fotuhi-Firuzabad M, Moeini-Aghaie M. Enhancing power system resilience through hierarchical outage management in Multi-microgrids. *IEEE Trans Smart Grid* 2016;7:2869–79.
- [24] Jalilpoor K, Oshnoei A, Mohammadi-Ivatloo B, Anvari-Moghaddam A. Network hardening and optimal placement of microgrids to improve transmission system resilience: a two-stage linear program. *Reliab Eng Syst Saf* 2022;224:108536.
- [25] Younesi A, Shayeghi H, Safari A, Siano P. Assessing the resilience of multi microgrid based widespread power systems against natural disasters using Monte Carlo Simulation. *Energy* 2020;207:118220.
- [26] Hou H, Wu W, Zhang Z, Wei R, Wang L, He H, et al. A tri-level Typhoon-DAD robust optimization framework to enhance distribution network resilience. *Reliab Eng Syst Saf* 2024;245:110004.
- [27] Sánchez-Pozo NN, Vanem E, Bloomfield H, Aizpurua JI. A probabilistic risk assessment framework for the impact assessment of extreme events on renewable power plant components. *Renew Energy* 2025;240:122168.
- [28] Nazemi M, Dehghanian P, Darestani Y, Su J. Parameterized wildfire fragility functions for overhead power line conductors. *IEEE Trans Power Syst* 2024;39: 2517–27.
- [29] Gao S, Wang J, Yu L, Zhang D, Zhan R, Kou L, et al. A multilayer bayesian network approach-based predictive probabilistic risk assessment for overhead contact lines under external weather conditions. *IEEE Trans Transp Electrification* 2023;9: 236–53.
- [30] Liu J, Tian L, Yang M, Meng X. Probabilistic framework for seismic resilience assessment of transmission tower-line systems subjected to mainshock-aftershock sequences. *Reliab Eng Syst Saf* 2024;242:109755.
- [31] Bessani M, Massignan JAD, Fanucci RZ, Camillo MHM, London JBA, Delbem ACB, et al. Probabilistic assessment of power distribution systems resilience under extreme weather. *IEEE Syst J* 2019;13:1747–56.
- [32] Liu X, Xie Q. A probabilistic framework to evaluate seismic resilience of substations based on three-stage uncertainty. *Reliab Eng Syst Saf* 2024;249:110219.
- [33] Dui H, Li H, Dong X, Wu S. An energy IoT-driven multi-dimension resilience methodology of smart microgrids. *Reliab Eng Syst Saf* 2025;253:110533.
- [34] Bianconi G. Multilayer Networks: Structure and Function 2018.
- [35] Jung C, Schindler D. Wind speed distribution selection – A review of recent development and progress. *Renew Sustain Energy Rev* 2019;114:109290.
- [36] Hou H, Xu T, Wu X, Wang H, Tang A, Chen Y. Optimal capacity configuration of the wind-photovoltaic-storage hybrid power system based on gravity energy storage system. *Appl Energy* 2020;271:115052.
- [37] Li W, Dong F, Liu J, Wang P, Zhao X. A three-stage decision-making study on capacity configuration of hydropower-wind-photovoltaic-storage complementary systems considering uncertainty. *Energy* 2024;313:134007.
- [38] Oboudi MH, Mohammadi M, Trakas DN, Hatzigaryiou ND. A systematic method for power system hardening to increase resilience against earthquakes. *IEEE Syst J* 2021;15:4970–9.
- [39] Baker J.W. An introduction to probabilistic seismic hazard analysis. White paper, version 2008;21:22.
- [40] Zeng Z, Fang Y-P, Zhai Q, Du S. A Markov reward process-based framework for resilience analysis of multistate energy systems under the threat of extreme events. *Reliab Eng Syst Saf* 2021;209:107443.
- [41] Panteli M, Pickering C, Wilkinson S, Dawson R, Mancarella P. Power system resilience to extreme weather: fragility modeling, probabilistic impact assessment, and adaptation measures. *IEEE Trans Power Syst* 2017;32:3747–57.
- [42] Zapata CJ, Silva SC, Burbano OL. Repair models of power distribution components. In: 2008 IEEE/PES Transm. Distrib. Conf. Expo. Lat. Am.; 2008. p. 1–6. 2008 IEEE/PES Transm. Distrib. Conf. Expo. Lat. Am.
- [43] Zhu Z, Zhou J, Yan C, Chen L. Power system operation risk assessment based on a novel probability distribution of component repair time and utility theory. In: 2012 Asia-Pac. Power Energy Eng. Conf.; 2012. p. 1–6. 2012 Asia-Pac. Power Energy Eng. Conf.
- [44] Bradley BA, Dhakal RP, Cubrinovski M, Mander JB, MacRae GA. Improved seismic hazard model with application to probabilistic seismic demand analysis. *Earthq Eng Struct Dyn* 2007;36:2211–25.
- [45] Zhang T, Xie M. On the upper truncated Weibull distribution and its reliability implications. *Reliab Eng Syst Saf* 2011;96:194–200.
- [46] Billinton R, Jonnavaithula S. A test system for teaching overall power system reliability assessment. *IEEE Trans Power Syst* 1996;11:1670–6.